Drug Delivery

http://informahealthcare.com/drd
ISSN: 1071-7544 (print), 1521-0464 (electronic)

Drug Deliv, Early Online: 1–16
 DOI: 10.3109/10717544.2014.887158

informa
healthcare

ORIGINAL ARTICLE

Microneedle-assisted microparticle delivery by gene guns: experiments and modeling on the effects of particle characteristics

Dongwei Zhang, Chris D. Rielly, and Diganta B. Das

Department of Chemical Engineering, Loughborough University, Loughborough, UK

Abstract

Microneedles (MNs) have been shown to enhance the penetration depths of microparticles delivered by gene gun. This study aims to investigate the penetration of model microparticle materials, namely, tungsten (<1 μm diameter) and stainless steel (18 and 30 μm diameters) into a skin mimicking agarose gel to determine the effects of particle characteristics (mainly particle size). A number of experiments have been processed to analyze the passage percentage and the penetration depth of these microparticles in relation to the operating pressures and MN lengths. A comparison between the stainless steel and tungsten microparticles has been discussed, e.g. passage percentage, penetration depth. The passage percentage of tungsten microparticles is found to be less than the stainless steel. It is worth mentioning that the tungsten microparticles present unfavourable results which show that they cannot penetrate into the skin mimicking agarose gel without the help of MN due to insufficient momentum due to the smaller particle size. This condition does not occur for stainless steel microparticles. In order to further understand the penetration of the microparticles, a mathematical model has been built based on the experimental set up. The penetration depth of the microparticles is analyzed in relation to the size, operating pressure and MN length for conditions that cannot be obtained in the experiments. In addition, the penetration depth difference between stainless steel and tungsten microparticles is studied using the developed model to further understand the effect of an increased particle density and size on the penetration depth.

Keywords

Gene gun, microneedle, microparticles, microparticle density, microparticle size, penetration depth, passage percentage

History

Received 13 December 2013
Revised 21 January 2014
Accepted 21 January 2014

Introduction

Gene gun systems have been designed primarily as needle-free techniques that can accelerate DNA-loaded microparticles to provide sufficient momentum so that they can breach the outer layer of the skin and achieve the purposes of gene transfection (Kendall et al., 2004; Walters & Roberts, 2007; Soliman, 2011; Kis et al., 2012). Generally, the epidermis layer of the skin is considered as the main target of these microparticles (Trainer & Alexander, 1997; Bennett et al., 1999; Quinlan et al., 2001; Liu, 2006; Soliman et al., 2011). However, cell and tissue damages are particular problems for the use of gene guns (Yoshida et al., 1997; Sato et al., 2000; Thomas et al., 2001; Uchida et al., 2009). In principle, reduction of the operation pressure in the gene guns (Yoshida et al., 1997; Uchida et al. 2009) and particle size can minimize the cell/tissue damage but these tend to decrease the particle momentum and, hence, the penetration depths of the microparticles in the tissue. In order to resolve these issues, a series of experiments that combine solid microneedles (MNs) with an in-house microparticle delivery system (see Figure 1) has been reported recently by Zhang et al. (2013a, 2014). The potential of a system that combines MNs and gene guns has been discussed in details by Zhang et al. (2013b).

MNs are minimally invasive microstructures that can pierce the outer layer of skin, namely the *stratum corneum*, almost painlessly, which has been shown to enhance drug delivery rate (Olatunji & Das, 2011; Donnelly et al., 2012; Nayak et al., 2013; Olatunji et al., 2013). They are generally classified into ''solid'' and ''hollow'' MNs (Al-Qallaf et al., 2009; Olatunji & Das, 2010; Olatunji et al., 2012; Nayak & Das, 2013; Han & Das, 2013; Zhang et al., 2013a,b). The solid MNs are able to penetrate the human skin to make holes (McAllister et al., 2003; Davis et al., 2004; Kalluri & Banga, 2011) as well as deliver drugs/genes that are coated (Cormier et al., 2004) or encapsulated (Miyano et al., 2005). The MN holes can also be used by the biolistic system for the delivery of the microparticles. In this case, the microparticles can penetrate with less resistance into the skin through the holes and further achieve an enhanced penetration depth to allow gene transfection in deeper tissue. Zhang et al. (2014) have used the experimental setup of MN-assisted microparticle delivery to fire biocompatible stainless steel microparticles having an average diameter of 18 μm into a skin mimicking agarose gel. Their results have shown that a number of microparticles penetrate through the holes and achieve a considerable increase in the maximum penetration depth, e.g. a penetration depth of 1272 ± 42 μm was achieved inside the gel using 1500 -μm-long

Address for correspondence: Diganta B Das, Department of Chemical Engineering, Loughborough University, Loughborough LE113TU, UK. E-mail: d.b.das@lboro.ac.uk

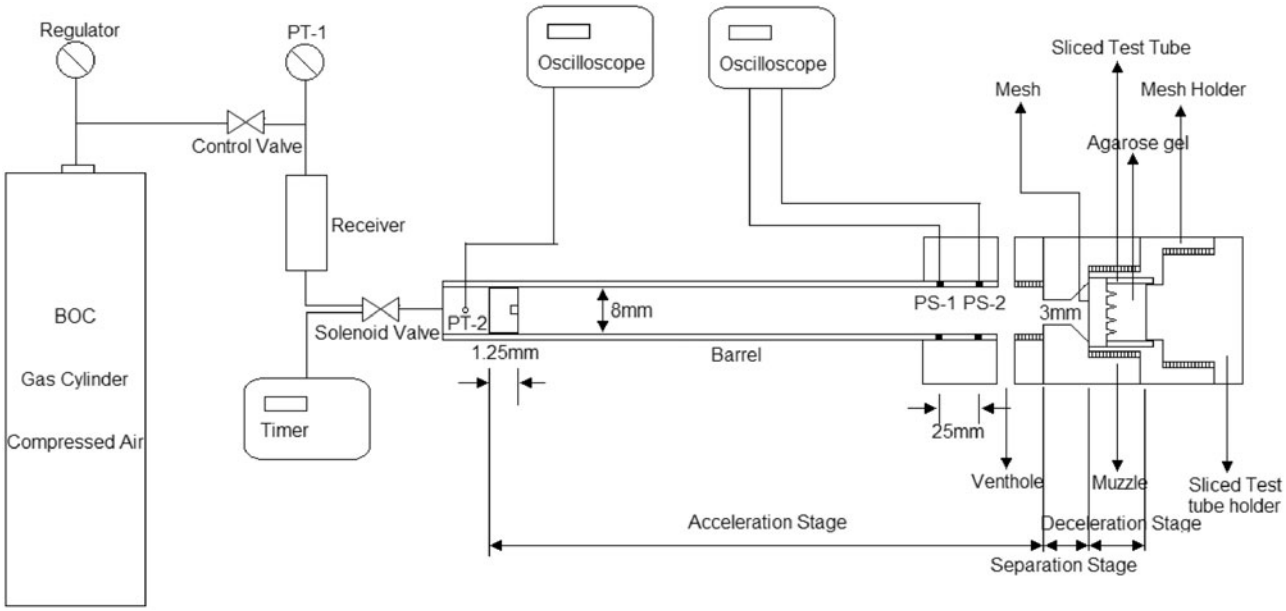

Figure 1. A schematic diagram of the experimental rig for the MN-assisted microparticle delivery system (Zhang et al., 2014).

MNs (AdminPatch MN 1500, AdminMed, Sunnyvale, CA) as compared to the cases where the same gel and operating conditions were used and yet little or no penetration of MNs was observed due to the absence of MNs.

The overall process of MN-assisted transdermal microparticle delivery from gene guns consists of three main stages, which are the acceleration, separation and deceleration stages (Zhang et al., 2013a, 2014). These stages are identified in Figure 1. As can be seen, the experimental setup stores the pressurized gas in a gas receiver to a desired pressure which is detected by a digital pressure transducer. The release of the pressurized gas is operated by a solenoid valve. In addition, it is worth mentioning that the system uses a ground slide that can prevent the impact of pressurized gas on the target tissue and release the gas from the vent holes in the barrel. The acceleration stage is a major part of the particle delivery process as it is within this stage the microparticles are accelerated to sufficient velocities using the pressurized gas as a driving source. To achieve these, the microparticles are compressed and bound loosely into a pellet form and loaded into a ground slide in the system (Figure 1). As the ground slide is accelerated by the pressurised gas, the pellet containing the microparticles is also accelerated. The separation stage is then followed, which is aimed at separating the pellet into individual particles by a mesh although it is possible that this stage produces a few agglomerates.

The deceleration stage involves two steps as follows: (i) the transport of the microparticles in a space between mesh and target and (ii) the penetration of microparticles into the chosen target. Previously, Zhang et al. (2014) used an experimental rig (Figure 1) to deliver stainless steel microparticles into a skin mimicking agarose gel so as to demonstrate the feasibility of MN-assisted microparticle delivery. The results have shown that an enhanced penetration depth of microparticles inside the agarose gel can be achieved using MN-assisted microparticle delivery at a much lower injection pressure compared to typical gene guns.

Generally, the route of the microparticle penetration in the target tissue is divided into two types, the extracellular and intercellular routes (Mitchell et al., 2003; Soliman & Abdallah, 2011; Zhang et al., 2013b). The extracellular route may occur with large particles due to failures between the cell boundaries (Soliman, 2011). For example, Mitchell et al. (2003) have fired stainless steel microparticles of 25 μm average diameter into canine buccal mucosa using light gas gun (Crozier & Hume, 1957), which is governed by the microparticle transport through extracellular route. However, the disadvantage is that large particle sizes may cause a lot of damage or destroy the skin surface.

The intercellular route is considered to be important in the case of delivering small particles, which pass through individual cell membranes, e.g. it can be used for particle-mediated DNA immunization (Hardy & Kendall, 2005; Soliman & Abdallah, 2011). Dense materials (e.g. gold and tungsten) are often made into small particles of a diameter ranging from 0.6 to 6 μm (Hardy & Kendall, 2005; Soliman, 2011) which are smaller than typical cell diameters. The particles can be accelerated to higher speeds to obtain enough momentum to breach the skin and penetrate through the individual cell membranes. Although gold is recommended for the particle delivery due to its high density, low toxicity and lack of chemical reactivity (Macklin et al., 2000), it is an expensive material. Several studies for the golden microparticles delivery have been made, which show that the gold microparticles can breach the human skin and penetrate to a depth ranging from 35 to 135 μm at 30 bar operating pressure (Giudice & Campbell, 2006; Arora et al., 2008). Kendall et al. (2004) used a convergent–divergent device to accelerate gold particles of 1.8 μm diameter, which achieve a maximum penetration depth of 78.6 μm in the skin at 60 bar pressure. Mitchell et al. (2003) found that gold particle of 1–3 μm diameter can reach a depth of around 60 μm in canine tissue at an injection particle velocity of 550 ± 50 m/s. Recently, O'Brien & Lummis (2011) reported that the penetration depth of golden microparticles of 1 μm diameter in mouse ear

tissue is 50 ± 11 μm when the Helios gene gun is used at an operating pressure of 5.1 bar (75 psi).

In general, the intercellular route is the preferred penetration route due to less cell and tissue damages for the small microparticles. In order to validate the effect of the MN-assisted microparticle delivery on the small microparticles, tungsten microparticles may be chosen to analyze the penetration in the skin mimicking agarose gel. Tungsten microparticles are considered to be a good substitute for golden microparticles for research of biolistic microparticle delivery because of their cost effectiveness compared to gold particles, despite the fact that they can be toxic to cells (Russell et al., 1992; Bastian et al., 2009; Yoshimisu et al., 2009). For example, Klein et al. (1987) first used a particle gun to accelerate spherical tungsten particles of 4 μm diameter into epidermal cells of onions. Williams et al. (1991) used a helium-driven apparatus to study 3.9 μm average diameter tungsten and of golden particles, with a diameter ranged from 2 to 5 μm, on mouse liver. Recently, the review paper by Zhang et al. (2013b) discussed the importance of particle characteristics and operation condition on the delivery of the microparticles in detail.

Motivated by the above work, this study aims to investigate the effects of particle characteristics on MN-assisted microparticle delivery by using microparticles (e.g. tungsten microparticles, biomedical grade stainless steel) of different densities and particle sizes. This study also gives an indirect comparison between the extracellular and intercellular routes using MN-assisted microparticle delivery. Zhang et al. (2013a) determined the passage percentage of stainless steel microparticles at various conditions, e.g. mesh pore size, polyvinylpyrrolidone (PVP - binder) concentration and operating pressure. They pointed out the required mesh pore size and PVP concentration of pellets for MN-assisted microparticle delivery for given particle size. This study aims to revisit the same questions to determine the dependence of particle characteristics using tungsten and stainless steel microparticles with the help of Zhang et al.'s (2014) experimental rig. A skin mimicking agarose gel is used as a target to determine the difference in penetration depth between tungsten and stainless steel microparticles. In order to further understand the particle size and density effect on the penetration depth, a mathematical model of MN-assisted microparticle delivery is built using MATLAB (Version R2012b). The mathematical model is used to analyze the theoretical penetration depth of those two materials of microparticles and further to verify the experimental results. In addition, the model aims to investigate the effect of a range of target properties (e.g. density, viscosity) on the maximum penetration depth of microparticles. The developed model is also used to determine the characteristics of the microparticle delivery where experimental data are not available. Please note that this study is focused on modeling the microparticle delivery process. The issues related to the loading of genes on these particles and subsequent gene transfection in a target cells are not discussed in this study.

Please note that most of the technologies for loading DNA onto the particles and delivering the DNA-loaded particles are well developed. In the present context, we do not propose any changes to these existing methods but suggest a modification where the particle delivery process/devices are coupled with MNs. The potential of these method are discussed in detail by Zhang et al. (2013a,b, 2014).

Materials and experimental methods

Materials

Irregular shaped tungsten microparticles were purchased form Sigma-Aldrich Company Ltd (Gillingham, UK). It is considered as a good replacement for gold particles, because its density is similar to gold and has a low cost (Menezes et al., 2012). Stainless steel mesh with pore size of 122 μm was obtained from Mesh, UK, Streme Limited (Marlow, UK). Irregular shaped and spherical biocompatible stainless steel microparticles were purchased from Goodfellow Cambridge Ltd. (Huntingdon, UK) and LPW Technology Ltd. (Daresbury, UK), respectively. Agarose powder (Sigma-Aldrich Company Ltd., Gillingham, UK) was used to prepare a skin mimicking agarose gel, which was used a target for the microparticles penetration experiments. Detailed method of preparation for this gel is given by Zhang et al. (2014).

Two different solid MN arrays that vary in the lengths of the MNs (AdminPatch 1200 and 1500) were purchased from nanoBioSciences limited liability company (Sunnyvale, CA). The MNs are distributed as a diamond shape (see Figure 2) on a 1 cm^2 circular area. In addition, an in-house fabricated MN array is used which consists of 750-μm-long MNs. The characteristic of each MN array is presented in Table 1. Although the results from the use of different MNs may be different, a range of dimensions of the MNs provide us the

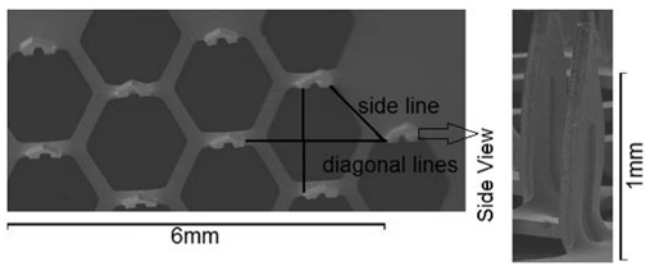

Figure 2. The image of AdminPatch 1500 (Note: MNs of AdminPatch 1200 are distributed as a diamond pattern) (Zhang et al., 2014).

Table 1. The characterizations of the MN array (Zhang et al., 2014).

MN name	Parameters	Value (μm)
Adminpatch MN 1500	Length	1500
	Width	480
	Thickness	78
	Space between MNs	1546
	Spaces on diagonal directions (see Figure 2)	1643
		3000
Adminpatch MN 1200	Length	1200
	Width	480
	Thickness	78
	Space between MNs	1252
	Spaces on diagonal directions	1970
		2426
In-house fabricated MN 750	Length	750
	Diameter	250
	Space between MNs	500

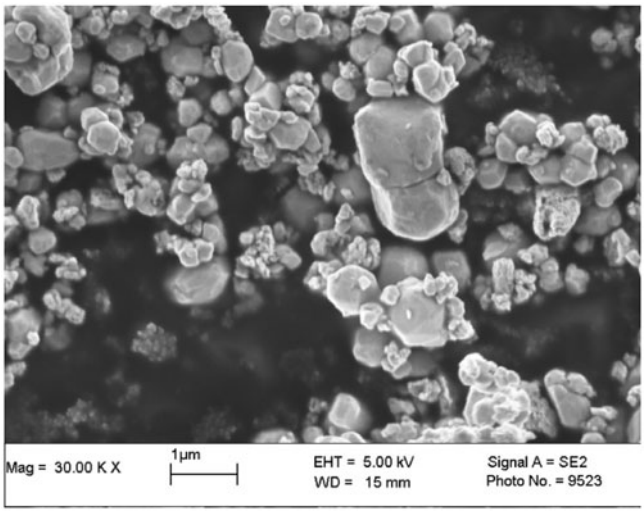

Figure 3. An SEM image of irregular tungsten powder (Sauter mean diameter: 0.49 μm).

opportunity to understand the effects of a geometric parameter more accurately. Therefore, we consider it to be important to use more than one MN in our experiments despite differences in their geometries.

Characterization of tungsten microparticles

The particle size distribution of tungsten powder is analyzed by a particle size analyzer (Mastersizer 2000; Malvern Instruments, Ltd, Malvern, Worcestershire, UK). It is found to range from 0.198 to 1.439 μm with a mean diameter of 0.58 μm and Sauter mean diameter of 0.49 μm. The particles can be viewed in the scanning electron microscopy (SEM) image in Figure 3. The tungsten particles are highly agglomerated and have rough surfaces. From the SEM image, 50 random microparticles are chosen to measure the average sphericity of the tungsten microparticles which is found to be 0.66 ± 0.13 μm. The average bulk density and porosity of tungsten powder are 7.43 ± 0.08 g/cm^3 and $59.6 \pm 0.4\%$. Ultimately, by combining the SEM image results with the size distribution, gained from particle size analyzer, it is possible to confirm that the tungsten particles are a nanosize powder.

Characterization of the pellet

For the MN-assisted microparticle delivery, the microparticles are required to be in the form a compressed cylindrical pellet which is prepared by a pellet press as described by Zhang et al. (2013a). Furthermore, the packing density should be homogeneous within the pellet as far as possible so as to increase the possibility that when the pellet is broken into particles, one obtains uniformly separated particles. This is an important characteristic of the developed process. Heterogeneity in the packing of the pellet is likely to create more uncertainty in the distribution of the separated particles. To prepare the cylindrical pellet, Zhang et al. (2013a) mixed 40 mg of PVP in 1 ml of ethanol in which an amount of 0.035 g stainless steel microparticles has been added and bind the particles together. The mixture is transferred to a pellet press (Zhang et al., 2013a) and compressed into a solid cylindrical pellet. Ethanol is evaporated due to their high volatility and therefore, it is not present in the dry pellet which is used in experiments. A similar method was followed to produce the pellets in this work. Furthermore, the homogeneity of the microparticle packing was checked using a microcomputed tomography (micro-CT). Micro-CT is an advanced non-destructive 3D imaging technique that can be used to clearly understand the internal microstructure of the samples (Ritman, 2004). Micro-CT has been used to detect any internal damage (e.g., internal fracture in the porous pellet) and/or heterogeneity in the packing of pellet in this work. As an example, a three-dimensional view of the stainless steel pellet is shown in Figure 4(A). As can be seen, the stainless steel microparticles are compressed into a homogenous cylindrical pellet with approximately 2 mm in diameter and length. Although the top and button surfaces of the pellet are slightly uneven because the pellet gets stuck on the pellet press, it is not a big concern as it seems that the packing density of the particles does not vary. The internal top view of the pellet at the position of 1.08 mm on the z axis is shown in Figure 4(B) and the size view of the internal structure of the pellet at the position of 1.08 mm on the y-axis is shown in Figure 4(C). It shows that PVP (white spots) is non-uniformly distributed in the pellet. PVP fills the void space in the microparticles causing them to bind loosely together as indicated by the white circles (PVP) in Figure 4(B,C). The above figures cannot clearly show the PVP combination of the pellet. Therefore, an SEM view is provided, which shows the top surface of a pellet (see Figure 5A).

Figure 5(A) clearly shows the characterization of the pellet top surface. As can be seen, the microparticles are bound to form a uniform pellet surface. As expected, the PVP is distributed nonuniformly around the pellet, which agrees with results detected by the micro-CT (Figure 4). Thus, it may cause the pellet to separate into a few agglomerates after the separation stage due to increased bind strength between some of microparticles. Previously, Zhang et al. (2013a) analyzed the passage percentage of the pellet and size distribution of the separated particles using various operating pressure and different binder (PVP) concentration. They showed that 40 mg/ml PVP in a pellet is ideal as it almost separates the pellet into individual microparticles with some small agglomerates using 178 μm pore size of mesh. As presented in Figure 5(B), the application of mesh pore size presents a good control of the size distribution of the separated microparticles and uses to the following experiments for the investigation of the penetration depth of tungsten microparticles in the skin mimicking agarose gel.

Modeling of MN-assisted microparticle delivery: governing equations

The detailed theoretical principle of each stage is discussed in the following sections.

Acceleration stage

For the MN-assisted microparticle delivery, a pellet is attached to a ground slide, which is accelerated by a pressurized gas in the acceleration stage (see Figure 1). It indicates that only the pressurized gas has done the work

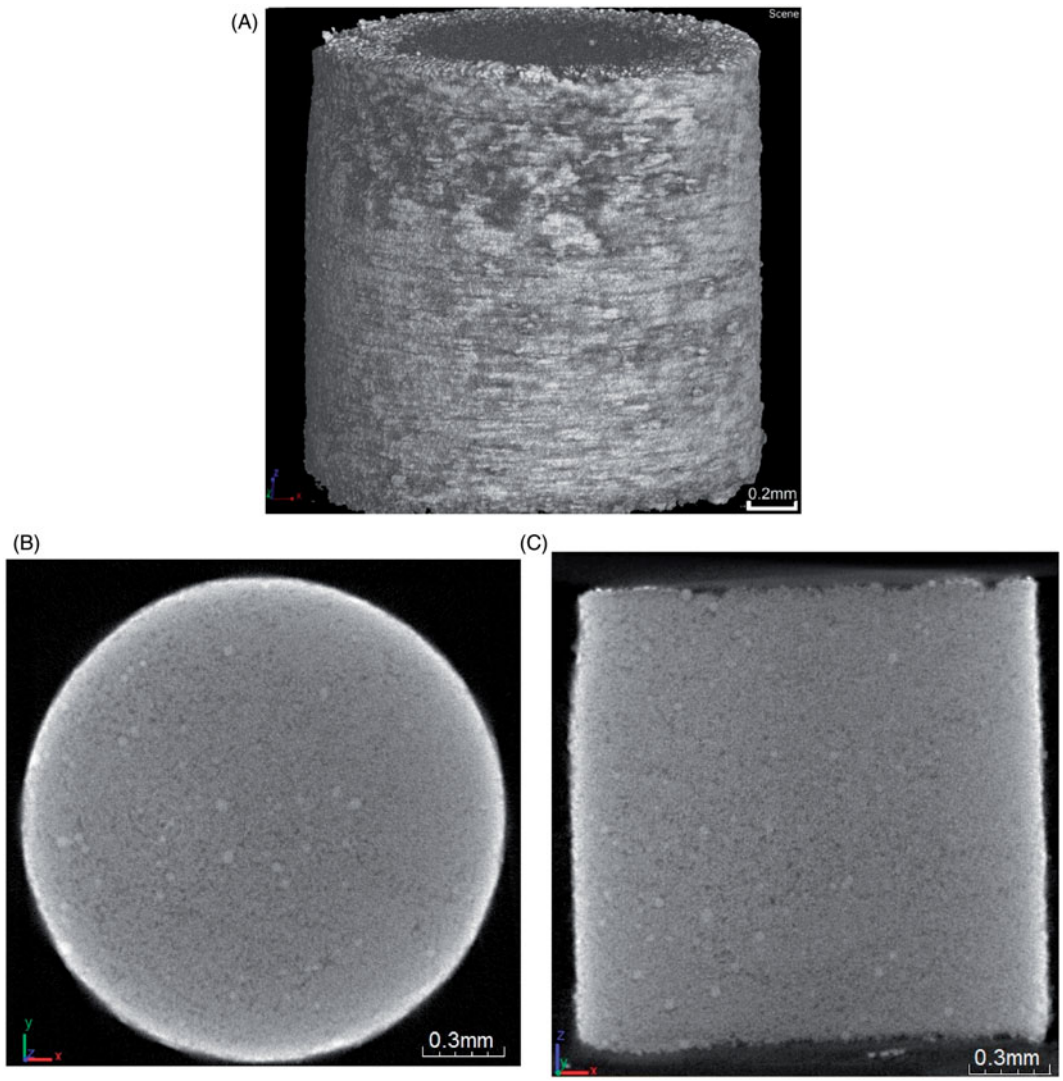

Figure 4. Micro-CT images of a stainless steel microparticle pellet made of 40 mg/ml PVP (white spots in the images): (A) reconstructed three dimension view of the pellet (B) top internal view across the pellet at the position of 1.08 mm on the z axis (C) side internal view across the pellet at the position of 1.08 mm on the y axis. The images show homogeneity of the packing of the microparticles.

during the acceleration process. The equation to describe this process:

$$E = \int_0^L P_2 \pi R^2 \, sdl \tag{1}$$

where E is the kinetic energy of the pellet, L is the traveling distance of the ground slide in the barrel before the pellet is broken into microparticles and R is the radius of the barrel. The gas pressure to push ground slide moving forward is P_2 which decreases from a pressure P_1 in front of the barrel. The gas expansion can be described by the Boyle's law (Webster, 1995) as below:

$$P_1 V_1^{\gamma} = P_2 (V_1 + V_2)^{\gamma} \tag{2}$$

where γ is the heat capacity ratio, which defines as a constant of 1.6 for monatomic gas or 1.4 for diatomic gas.

The kinetic energy of the pellet attached ground slide at the end of the barrel can also be calculated as:

$$E = \frac{1}{2} M u^2 \tag{3}$$

where M is the mass of the pellet attached ground slide and u is the velocity of the ground slide.

From an energy conservation point of view, the ground slide velocity can be specified as follows:

$$u = \sqrt{\frac{2P_1 V_1^{\gamma} [(V_1 + \pi R^2 L)^{1-\gamma} - (V_1)^{1-\gamma}]}{M(1-\gamma)}} \tag{4}$$

Separation stage

In theory, the pellet is released from the ground slide at end of the barrel and separated by a mesh in the separation stage. Let us assume that the pellet has a mass of m_p and it is separated into n microparticles with the same mass m and they have the same velocity u_1 after passing through the mesh. Furthermore, the energy loss is assumed to be x in the process of the pellet separation. According to the energy conservation law, to describe the kinetic energy of the separated microparticles which is given as:

$$\frac{1}{2} n m u_1^2 = (1-x) \times \frac{1}{2} m_p u^2 \tag{5}$$

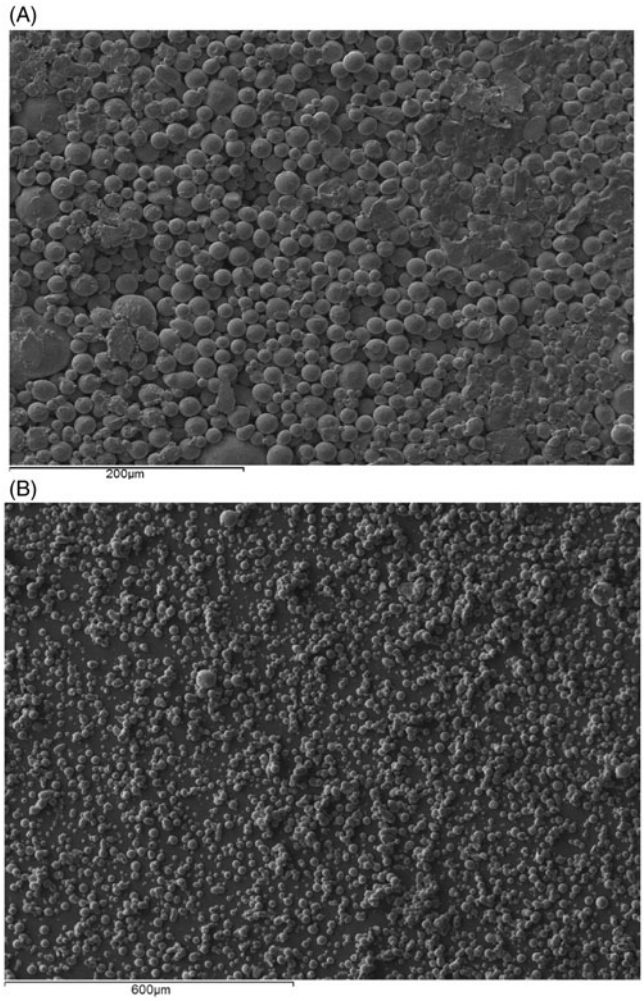

Figure 5. (A) SEM image of the top surface of the pellet (B) SEM image of the separated microparticles from a pellet which is made of 40 mg/ml PVP concentration and fired at a pressure of 20 bar and separated using a mesh of 178 µm pore size.

Equation (5) can be rearranged to an equation that is used to calculate the velocity of the separated microparticle and gives as:

$$u_1 = \sqrt{1-x} \times u \tag{6}$$

Deceleration stage

The deceleration stage of the microparticles is an important stage that directly affects the penetration depth of microparticle in the skin. The drag force of the skin is the major factor to decelerate the microparticles. In this study, the particle penetration in the skin use Newton's second law to proportional the change rate of particle momentum to the drag force f_d:

$$f_d = -m\frac{du_d}{dt} \tag{7}$$

where f_d is the drag force acting on the microparticles, u_d is the velocity of microparticles.

Various studies have adopted that the drag force acting on the microparticles is split into a yield force (F_y), a frictional resistive force (F_f) and a resistive inertial force of target material (F_i) (Dehn, 1987; Kendall et al., 2001; Mitchell et al., 2003; Liu, 2007; Soliman et al., 2011). Thus, Equation (7) is written as:

$$-(F_i + F_f + F_y) = m\frac{du_d}{dt} \tag{8}$$

The equations for each resistant force are shown as below:

$$F_i = 6\pi\mu_t r_p u_4 \tag{9}$$

$$F_f = \frac{1}{2}\rho_t A_c u_4^2 \tag{10}$$

$$F_y = 3A_c\sigma_y \tag{11}$$

where μ_t is the viscosity of the target, r_p is the radius of the microparticle, ρ_t is the density of the target and σ_y is the yield stress of the target.

Modeling strategy and parameters

For the purpose of this study, we use the software MATrix LABoratory (Matlab) to build and solve the theoretical model for MN-assisted microparticle delivery. The model consists of three main parts including a main program, an event program and two function programs (acceleration and deceleration stage). The main program simulates the whole process of the MN-assisted microparticle delivery. The event program defines the impact points of the microparticles on the skin, rebound points on the boundary of the gap between mesh and skin and the end points inside the skin. The function programs input the equations, which are used to determine the theoretical results. The function programs are implemented to the main program by choosing a suitable *ode* solver which requires considering the condition of the function program (stiff/non-stiff). In addition, an *if* statement has been used to define the position of the microparticles and further to confirm the selection of the equations to calculate the theoretical velocity of microparticles at different position. A *for* statement has been used to repeat the simulation of a number of microparticles in the deceleration stage.

In the model, human skin is considered as a target for microparticles in the model. The three main layers of human skin, stratum cornum, viable epidermis (VE) and dermis layers are considered in the model. The detailed skin properties are listed in Table 2. It is worth to mention that the yield stress and density of the dermis layer is considered the same with the VE layer. Zhang et al. (2014) used porcine skin instead of human skin to analyze the viscosity by using a rotational viscometer with parallel plate geometry. The result will be used in this study, which is shown in Table 2. The viscosity of each skin layer is treated as the same in the model.

The lengths of the pierced holes are obtained from measuring the hole lengths in the skin mimicking agarose gel when MNs are inserted. In this case, this model is chosen to analyze the delivery of tungsten microparticles. Zhang et al. (2014) indicated that the pellet is separated into individual particles with a few agglomerates using a mesh and then penetrates into the target. It illustrates that a number of the tungsten particles agglomerated after the separation stage

Table 2. Skin properties used in the model.

Parameter	Value	Reference
Thickness of viable epidermis (VE), T_{ve} (m)	0.0001	Holbrook et al. (1974); Matteucci et al. (2009); Schaefer & Redelmeier (1996)
Thickness of stratum cornum(SC), T_{sc} (m)	0.00002	
Yield stress of SC, Y_{sc} (MPa)	3.2–22.5	Wildnauer et al. (1971)
Density of SC, ρ_{sc} (g/cm^3)	1.5	Duck (1990)
Density of VE, ρ_{ve} (g/cm^3)	1.15	Duck (1990)
Yield stress of VE, Y_{ve} (MPa)	2.2	Kishino & Yanagida (1988)
Viscosity of skin, μ_t (Pa s)	19.6	Zhang et al. (2014)

Table 3. Relevant constants used in the developed model.

Parameter	Value
Mass of ground slide with the pellet, M (g)	1.25
Length of barrel, L (m)	0.5
Radius of barrel/ground slide, R (m)	0.00375
Volume of receiver, V_1 (L)	1
Space between mesh and skin, L_1 (m)	0.05
Density of tungsten (g/cm^3)	19.25
Density of stainless steel (g/cm^3)	8
Average diameter of tungsten particle (μm)	3
Average diameter of spherical stainless steel particle (μm)	18
Average diameter of Irregular stainless steel particle (μm)	30
Viscosity of air, μ (Pa s)	1.78
Length of pierced holes, L_p(μm)	
Adminpatch 1500	1149
Adminpatch 1200	1048
In-house fabricated MN	656
Width of pierced holes L_w (μm)	
Adminpatch 1500	302
Adminpatch 1200	302
In-house fabricated MN	156

in the experiment. In order to correlate the model with the realistic experiments, a number of tungsten microparticles are considered to the diameter of tungsten particle are considered to agglomerate together to be 3 μm diameter after the separation stage in the model. Previously, Zhang et al. (2013a, 2014) analyzed the sauter diameter of the spherical and irregular stainless steel using a particle size analyzer of Coulter. They also measured the average length of pierced holes in the skin mimicking agarose gel using a digital optical microscope. The length is considered uniformly and applied to the model in this case. The detailed set up of the particles properties and other relevant constants used in the model are listed in Table 3.

Results and discussions

The purpose of this section is to compare tungsten microparticle with stainless steel microparticles for the MN-assisted microparticle delivery based on the analysis of the passage percentage and the penetration depth inside target. The maximum penetration depth of microparticles is analyzed in relation to the operating pressure (see the Effect of the Operating Pressure section) and MN length (see the Effect of the MN Length section). In addition, a theoretical model is used to analyze the penetration depth in relation to above two parameters to compare tungsten particle with stainless steel microparticle and then to further understand the effect of particle density on microparticle penetration.

Analysis of passage percentage

In a previous study, Zhang et al. (2013a) showed that stainless steel microparticles yield a higher passage percentage and a good quality size distribution of separated microparticles if 40 mg/ml PVP (binder) concentration and a mesh with pore size of 178 μm are used. Here, the pellets of tungsten microparticles are operated at the same conditions as the previous study of the stainless steel microparticles and to make a comparison of the passage percentage between those two microparticles. The passage percentage is analyzed in relation to the operating pressure which is varied from 2.4 to 4.5 bar. As shown in Figure 6, the passage percentage is increased due to an increase in the operating pressures for each microparticle. This is because the pellets gain more momentum at higher operating pressures, which in turn also causes the separated particles to gain more momentum while passing through the mesh. Zhang et al. (2013a) indicated that the passage percentage of stainless steel microparticles reaches a maximum due to some particles sticking to the mesh and some rebounding, hence not passing into the test tube (particle collector). As expected, the tungsten microparticles show a similar performance to stainless steel. Figure 6 shows that the passage percentage of tungsten microparticles is less significant than stainless steel microparticles. It might be the size of the tungsten particles, too small, which causes the velocity of the separated particles to decrease faster after passage through the mesh and travel in air and stick on the mesh or the gap between mesh and target except the agglomerates.

Experimental analysis of the penetration depth of microparticles

Effect of the operating pressure

The operating pressure is shown to be a key variable on the penetration depth of stainless steel microparticles of 18 and 30 μm average diameters by us in a previous study (Zhang et al., 2013a, 2014). In this study, we aim to investigate the difference of the penetration depth between the larger stainless steel microparticle and smaller tungsten microparticles at various pressures. The tungsten microparticles cannot penetrate into the skin mimicking concentration of agarose gel. This is because the momentum of the particles is insufficient to breach the surface of the gel. In the experiment, the operating pressures are kept between 3 and 5 bar, which are low for the small particles to achieve velocity to breach the target. It requires a higher pressure for the small particles

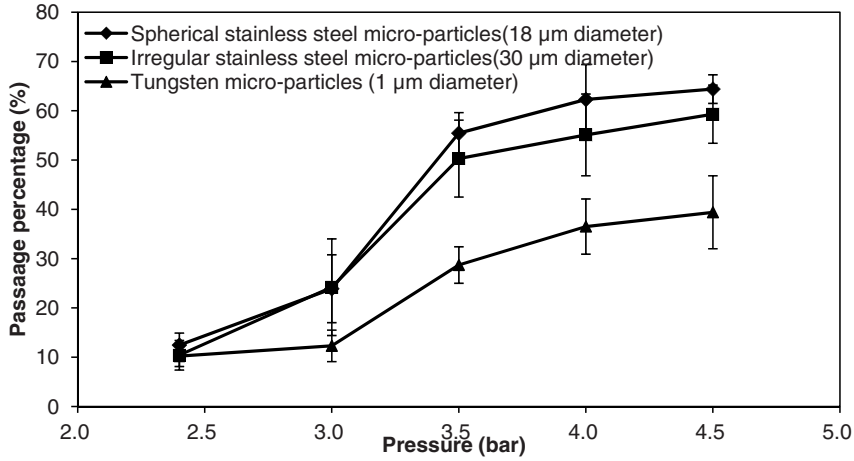

Figure 6. The effect of operating pressure on the passage percentage of the pellet separation. Each curve in the figure is generated from three repeats of experiments (mesh pore size: 178 μm, PVP concentration: 40 mg/ml).

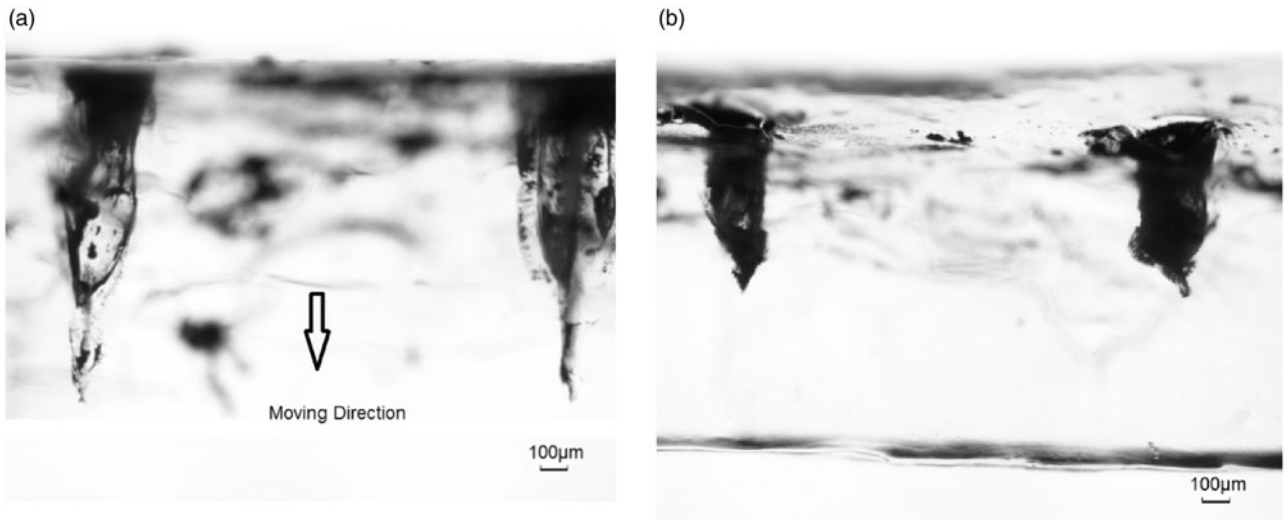

Figure 7. The effect of the operating pressure on the penetration depth of different type of particles (mesh: 178 μm of pore size: dash line: particle penetration without using MN; solid line: particle penetration with MN). Each curve in the figure is generated from three repeats of experiments.

to achieve sufficient momentum to penetrate further into the target. In addition, a comparison between tungsten and stainless steel microparticles is shown in Figure 7. As can be seen, both irregular and spherical stainless steel particles of 30 and 18 μm average diameters achieve good penetration depths inside the skin mimicking agarose gel. Although the density of the stainless steel is lower than tungsten, larger diameters of stainless steel microparticles increase their masses which lead to increased momentums of the microparticles so as to allow them to penetrate further in the target (skin mimicking agarose gel). The two microparticles show that the penetration depths increase due to an increase in the particle size.

To further understand the effect of the particle density and size on the penetration depth in the target, the theoretical model is used to analyze the penetration of above two materials of microparticles in a same target, which is discussed in the Effect of the Operating Pressure and Particle Size on the Penetration Depth section. When the MNs are inserted into the skin, it creates holes which remain there after the removal of the MNs. The microparticles can be delivered through these holes, thus compensating for the insufficient momentum. As presented in Figure 7, the penetration depths of the tungsten particles are greater inside the agarose gel when Adminpatch MN 1500 is used. This is because a number of particles can penetrate through the pierced holes. However, the maximum penetration depths of the microparticles vary while the pressure increases from 3 to 5 bar. Zhang et al. (2014) indicated that the length of the pierced holes is unable to maintain constantly, which varies the maximum penetration depth of the microparticles inside the target. Thus, the variation in the length of the pierced holes directly affects the penetration depth of the microparticles. It means that the holes length is a major factor to maximize the penetration depth in the MN-assisted microparticle delivery. The effect of MN length on the microparticle penetration depth is discussed in the Effect of the MN Length section in detail. Figure 7 also shows that the penetration depths of those two stainless steel microparticles are more than the tungsten microparticles. It indicates that an increased momentum due to increase in particle size/operating pressure of microparticles affect the penetration depth in the MN-assisted microparticle delivery.

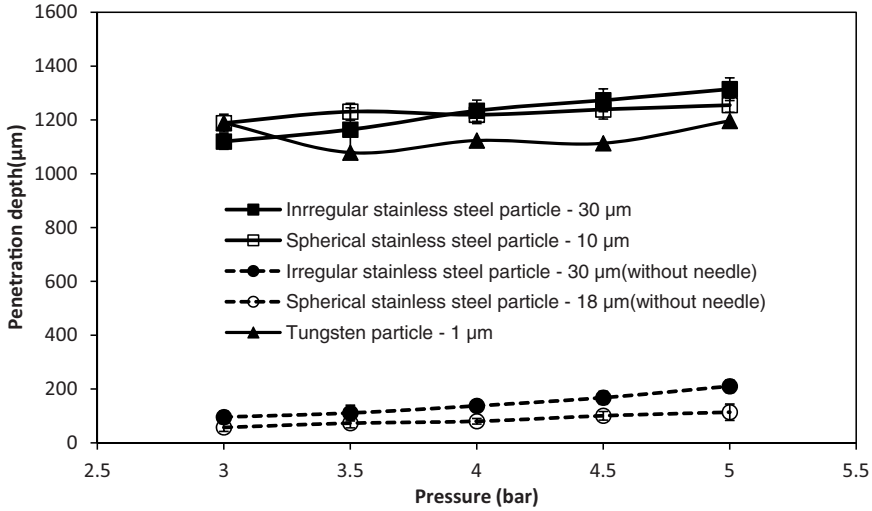

Figure 8. The penetration of tungsten microparticles in the skin mimicking agarose gel based on the assistance of MNs. (A) Adminpatch MN 1500, (B) in-house fabricated MN 750.

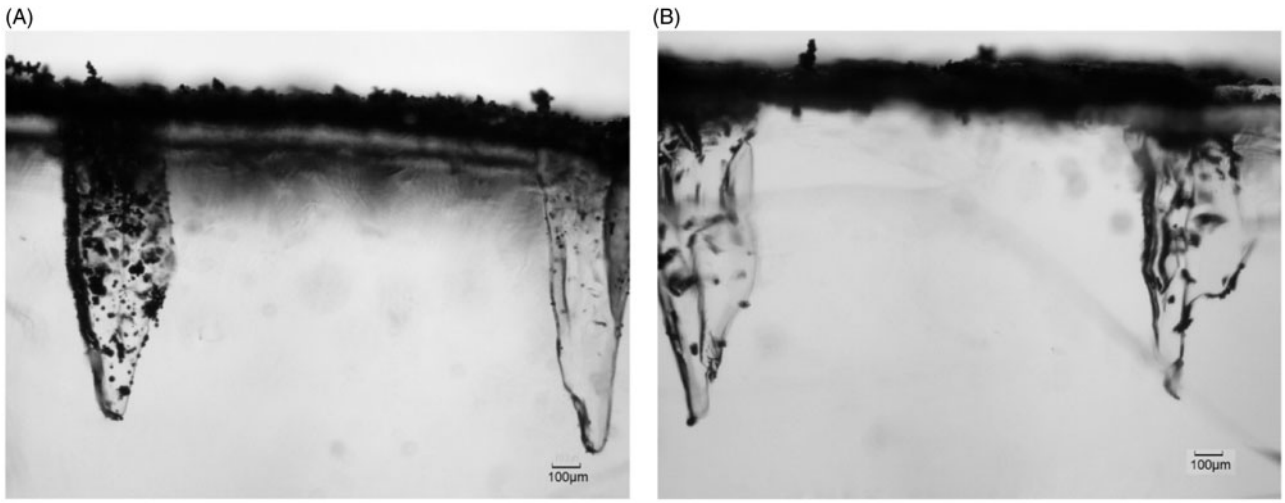

Figure 9. The penetration of stainless steel microparticles in the skin mimicking agarose gel based on the assistance of MNs. (A) Spherical microparticles of 18 μm average diameters, (B) irregular microparticles of 30 μm average diameters.

Effect of the MN length

Zhang et al. (2014) used three different lengths of MNs to study the maximum penetration depth differences of stainless steel microparticles of 18 and 30 μm diameters in a skin mimicking agarose gel. The characterizations of those three MNs are presented in Table 1. To further determine the effect of MN length on the penetration depth of small and dense microparticles, those three MNs are used in this case. Figures 8(A,B) show the penetration of the tungsten microparticles in the skin mimicking agarose gel based on the assistance of Adminptach MN 1500 and the in-house fabricated MN 750, respectively. As can be seen, the maximum penetration depth of microparticles after using Adminptach MN 1500 is more than that in in-house fabricated MN 750, but the number of microparticles entering the pierced holes is less obvious. This is because a long needle increases the length of pierced holes in the agarose gel, which maximizes the penetration depth of microparticles. In addition, the diameter of the in-house fabricated MN is greater than the thickness of the Adminptach MN 1500 MN (see Table 1), which creates wider holes to provide the convenience for particle penetration. It indicates that a desired penetration depth and amount of microparticles can be controlled by changing the MN length and width for further research.

Zhang et al. (2014) fired spherical and irregular stainless steel microparticles in the skin mimicking agarose gel. As presented in Figure 9, a number of microparticles penetrated further through the pierced holes. It presents the same effect with the tungsten microparticles. However, the amount of the stainless steel microparticles that penetrates into the pierced holes is less than tungsten microparticles if compared with the result in Figure 8. The number of irregular stainless steel microparticles of 30 μm average diameter is less than spherical microparticle (18 μm diameter) in Figure 9. It indicates that the amount of microparticle in the pierced holes decreases with increase in particle size. This is because of the reformation of the hole after the removal of the MN, reduced the opening area of the hole on the top gel surface and further to affect the microparticle penetration. Zhang et al. (2014) showed that the thickness of the hole is only 78 μm after the removal of Adminpatch MN 1500. It limits the amount of the microparticles to penetrate into the holes, especially to the

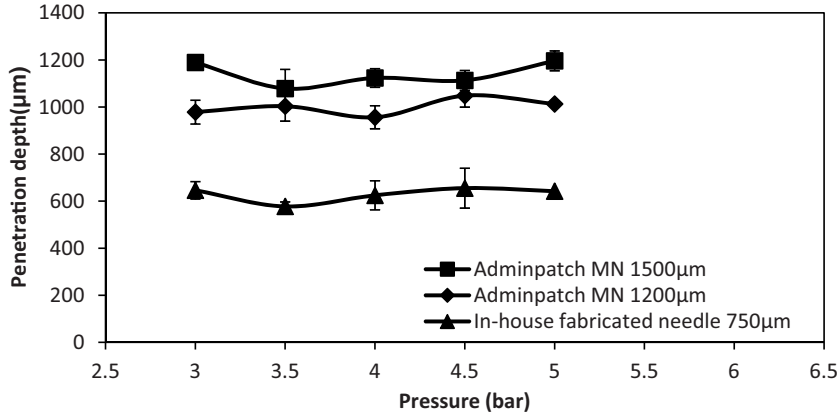

Figure 10. The maximum penetration depth of tungsten microparticles in the skin mimicking based on the assistance of MNs (mesh pore size: 178 μm; each curve in the figure is generated from three repeats of experiments).

large size of irregular stainless steel microparticles. However, the maximum penetration depth of each microparticle is close but related to length of the pierced holes.

The maximum penetration depths of tungsten microparticles show significant differences between each MN array as shown in Figure 10. It increases from an increase in MN length. As expected, a longer MN increases the length of the pierced holes and thereby increases the maximum penetration depth of microparticles. However, the maximum penetration depth is varied at different operating pressure. This is because the length of the pierced holes is varied after the removal of the MN array. The above results show the advantage of MN-assisted microparticle delivery which provides a positive effect on the particle penetration even if the momentum of the particle is insufficient to breach the target.

Modeling the penetration of microparticle in skin

First, this section aims to understand the MN-assisted microparticle delivery based on the modeling of the trajectory of tungsten microparticles in the deceleration stage. It is worth to mention that the tungsten microparticle and stainless steel microparticle may vary in shape and size which may affect results in reality. However, the both the stainless steel and tungsten, microparticles are assumed to be spherical with uniform size (average diameter) in the model. The maximum penetration depth is analyzed in relation to the operating pressure, MN length, particle size and density to further understand the difference between tungsten and stainless steel microparticles for the MN-assisted microparticle delivery. Finally, a further analysis of the effect of each resistive force on the maximum penetration depth of microparticles is discussed to verify the main factor that minimizes the penetration depth.

Modeling the delivery of tungsten microparticles

Figure 11(A) shows the trajectories of increased diameter of tungsten microparticles in the deceleration stage. The initial positions of the microparticles are randomly selected at the beginning to mimic the separation of the pellet of tungsten microparticles. In this case, we assumed that a number of tungsten microparticles are stuck together where the microparticles are spherical in shape and each microparticle has diameter of 3 μm after the separation stage (mesh). The trajectory is considered to be linear. The velocity decrease is represented by the colour change of the trajectory which corresponds to the colour bar in the figure. The velocity decreases slowly from approximately 135 to 110 m/s from the mesh to the target. Figure 11(A) shows that a number of the microparticles achieve further penetration depths via the pierced holes. The figure presents the similar performance of the developed model with experimental results. The detailed penetration process of tungsten microparticles in the skin is shown in Figure 11(B,C). Figure 11(B) shows the penetration of tungsten microparticles in the top skin layer of stratum corneum at 5 bar operating pressure. As can be seen, the particle velocity deceases very fast in the stratum corneum due to an increased resistance; the penetration depth is approximately 0.7 μm, which could be ignored. Some particles are delivered through the pierced holes and then penetrate into the epidermis/dermis layer of the skin (side surface of the pierced holes), as shown in Figure 11(C). It shows that the variation of the velocity is changed slightly in the pierced holes and decreased fast after penetrating the skin. It shows a similar performance as the penetration in the stratum corneum due to an increased resistance. Based on the above figures, the penetration depth of tungsten microparticles is negligible in the skin, which matches well with the experimental results.

Effect of the operating pressure and particle size on the penetration depth

In the experimental results, the operating pressure only presents a slight effect on the penetration depth of the tungsten microparticle without using MN. The pressures are varied from 3 to 5 bar, which are too low for small microparticles when compared with previous gene gun research (Mitchell et al., 2003; Kendall et al., 2004; Giudice & Campbell, 2006; Arora et al., 2008). In order to further understand the effect of the operating pressures on the penetration depth of this tungsten microparticle, the penetration depth is analyzed at various operating pressures which range from 3 to 60 bar in the model. As presented in Figure 12, the penetration depth of the tungsten particle is increased from 0.04 to 0.28 μm without using MNs while the pressure varies from 3 to 60 bar. The penetration depth is negligible. It illustrates that the tungsten particle of 3 μm diameter are too small for penetration even if the operating pressure increases to a great value. Figure 12 also shows that

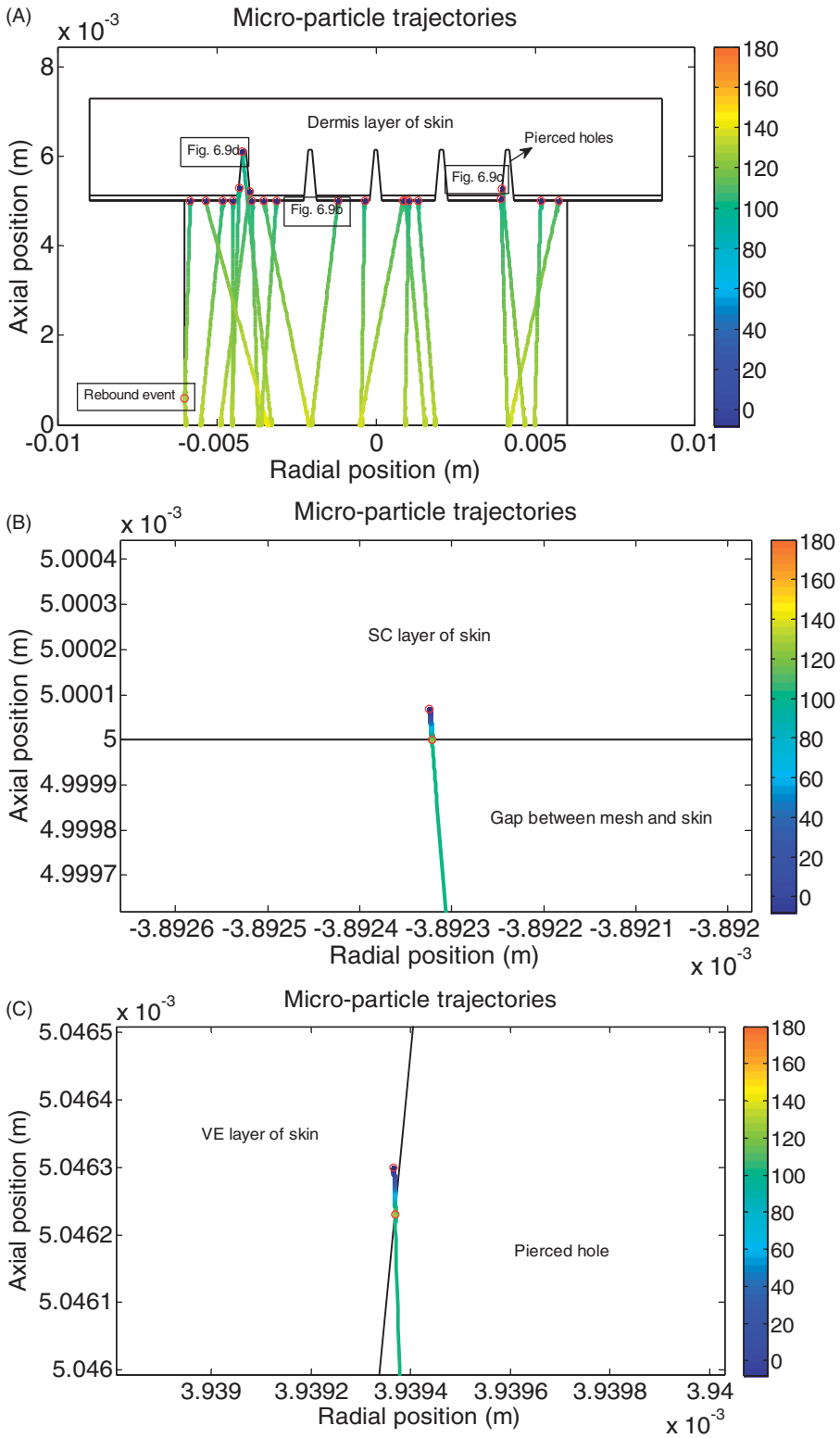

Figure 11. The trajectories of the tungsten microparticles in the deceleration stage. (A) The overall view of the microparticle trajectories. (B) The particle penetration at the area without needle hole. (C) The view of the microparticle penetrate through the needle hole (pressure: 5 bar).

the tungsten particle achieves a great penetration depth after using MNs. However, the penetration depth is increased slightly from an increase in operating pressure.

To further understand the effects of particle size and density on the penetration depth, the particle is assumed to be spherical in shape with uniform size and the particle diameter is varied from 3 to 100 µm for both stainless steel and tungsten microparticles using the presented model. As presented in Figure 13, the penetration depth of tungsten microparticles increases from 0.07 to 65.61 µm in the skin without using MNs and from 1149.07 to 1214.61 µm using Adminpatch MN 1500 at 5 bar pressure. It shows more penetration depth than stainless steel, which only penetrates 0.02 to 17.36 µm in the skin and 1149.02 to 1170.5 µm using a same MN as tungsten while the particle diameter ranges from 3 to 100 µm. This comparison directly shows the advantage of dense particles on the penetration in the target for gene gun systems.

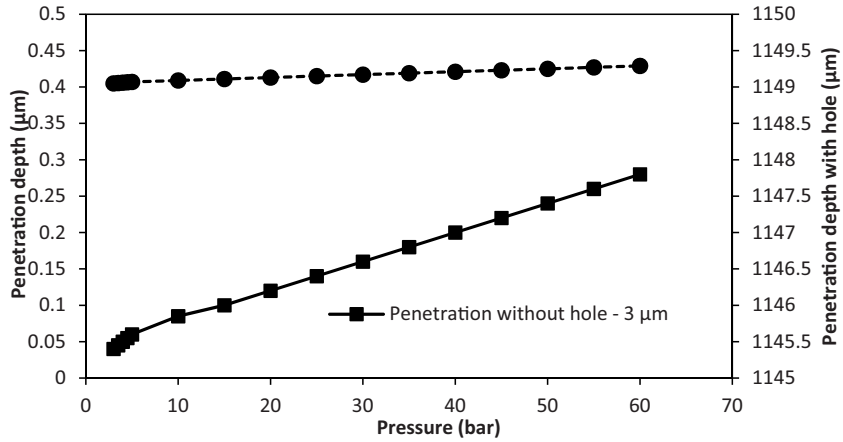

Figure 12. The effect of the operating pressure on the penetration of tungsten particle.

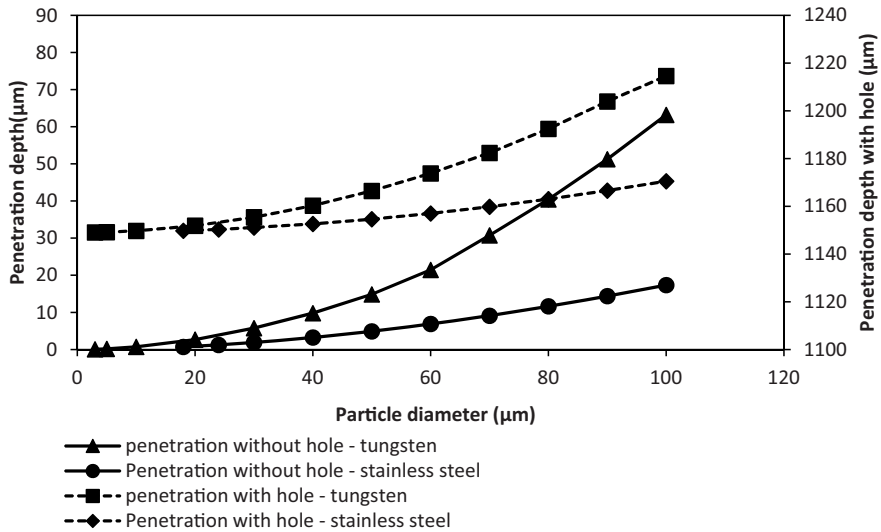

Figure 13. The effect of the tungsten particle size on the penetration depth (operating pressure: 5 bar).

A comparison of the penetration depth of the tungsten microparticles (3 μm) between model and experimental results is shown in Figure 14. It is worth to mention that the difference between experiment and modeling may be due to the assumption that the particle shape of the tungsten particle is regular after the separation stage in the model. As can be seen, the tungsten particles penetrate less than 0.1 μm without using MN for the model result. It matches well with the experimental results, which show that the tungsten microparticles cannot penetrate into the skin mimicking agarose gel. However, this condition can be made up by using MNs. As presented in Figure 14, the tungsten microparticles reaches a further depth using Adminpatch MN 1500, but the maximum penetration depths are varied at pressure ranges from 3 to 5 bar. This is because it is not possible to ensure that the length of the pierced holes is constant each time using the same MN. As expected, the model results match well with the experimental results. In conclusion, the maximum penetration depth of tungsten microparticles is directly related to the length of the pierced holes, and the operating pressure only presents a slight effect on the penetration depth in this case. To further understand the effect of pierced holes on the penetration depth of tungsten microparticles, three different lengths of MNs (see Table 1) have been used and discussed in the following section.

Effect of the MN length

In the real experiments, some tungsten microparticles may be agglomerate after the separation stage. However, any effects of the particle agglomeration on the model results are not accounted for directly at this moment. This may be the reason why there are some differences between the experimental and modeling results; however, all comparison have produced reasonable match between the experimental and modeling results. Zhang et al. (2014) showed that the length of pierced holes has a greater effect on the maximum penetration of stainless steel particles, which is related to the MN length. As expected, it agrees with the results of tungsten microparticles shown in Figure 15. As can be seen, the maximum penetration depth of tungsten microparticles seems to be increased with an increase in the MN length. In principle, the length of pierced holes is directly related to the MN length, which maximizes its length. An increased length of the pierced holes allows a number of microparticles which deliver into the holes to penetrate further inside the target and maximizes the penetration depth. As expected, the experimental results are varied for each application of MNs due to difficulties maintaining a constant hole length. However, the model results match well with the experimental results, which illustrate the applicability of the model for MN-assisted microparticle delivery.

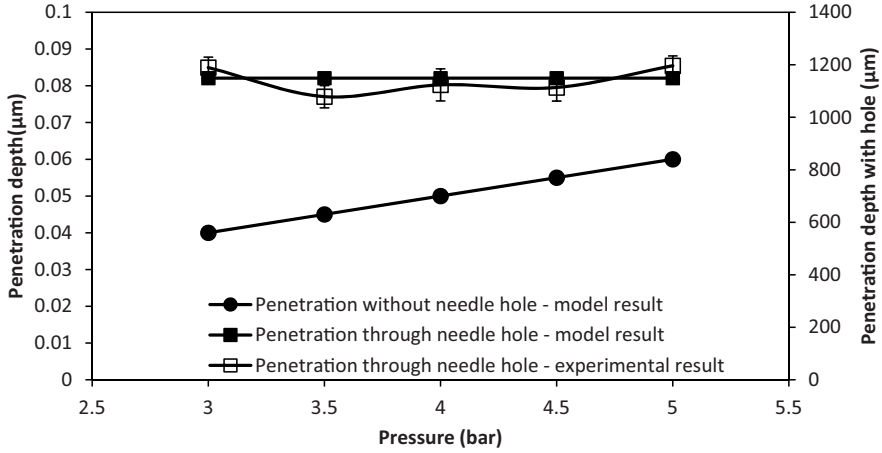

Figure 14. A comparison of penetration depth between model and experimental results (particle type: tungsten microparticle of 3 μm diameter). The experimental results in the figure are generated from three repeats of experiments.

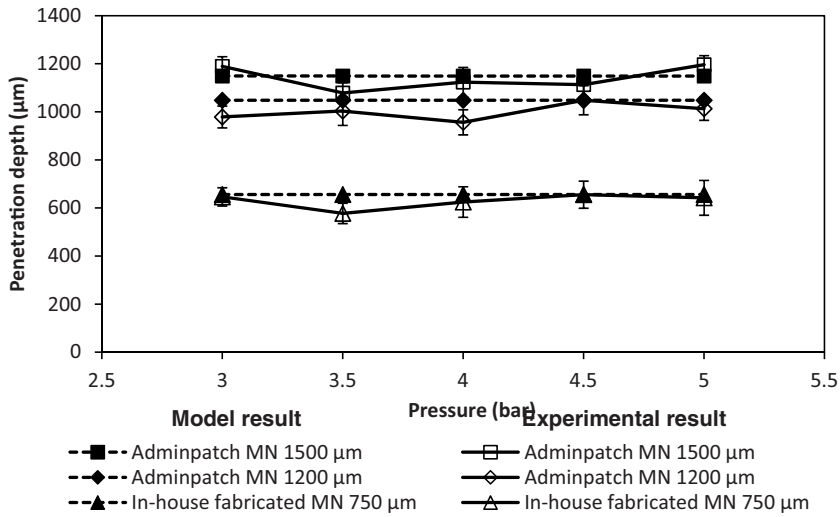

Figure 15. The effect of the microneedle length on the maximum penetration depth of the tungsten particle (operating pressure: 5 bar; particle type: tungsten microparticle of 3 μm diameter). The experimental results in the figure are generated from three repeats of experiments.

Dependence of particle penetration depth to particle size and density in relation to the resistive forces in the dermis layer of the human skin

The skin properties vary with one person to another (e.g. gender, age, race and various anatomical areas of the body of the same person (Vexler et al., 1999; Xu et al., 2007). As discussed earlier, the penetration depth of microparticles is related to the yield force (F_y), a frictional resistive force (F_f) and a resistive inertial force of target material (F_i), which decelerate the high-speed microparticles inside the target (see Equation 8). However, the yield force depends on the yield stress of the target (Equation 11). Furthermore, the resistive inertial force is related to the target viscosity (Equation 9) and the frictional resistive force depends on the density of the target material (Equation 10). In view of these inter-dependencies which in turn affect the microparticle delivery, this section aims to analyze the effects of each force on the penetration depth of microparticle to further investigate the major factors that provide a greater effect on the penetration depth.

For the MN-assisted microparticle delivery, the main point is the maximum penetration depth of the microparticle in the skin. As discussed already, a number of the microparticles penetrate through the holes made by the MNs to the dermis layer of the skin. In order to investigate the effect of each force on the maximum penetration depth of microparticle, we assume that the microparticles penetrate into the dermis layer at the tip area of the hole to obtain the maximum penetration depth of microparticles. In addition, we kept one of those three resistive forces as constant and ignored the other two forces to analyze the variation of the penetration depth in the model. As shown in Figure 16, stainless steel microparticles penetrated further than the tungsten particles due to the difference in particle size. Figure 16 also shows that the frictional resistive force provided a minimum effect on the microparticle penetration. The effect of the yield force on the penetration depth is greater than the frictional resistive force. However, the major factor is the resistive inertial force that causes the penetration depth of microparticles almost negligible if the hole length (1149 μm) is subtracted.

As discussed earlier, the resistive inertial force is a major component that determines the penetration depth of microparticles for the gene gun-based microparticle delivery. Target viscosity directly affects the resistive inertial force. In order to further understand the effect of the resistive inertial force on the particle maximum penetration depth, the theoretical model is used to simulate the effect of varying the viscosity of the dermis layer from 5 to 19.6 MPa where we kept the yield stress and density (see Table 2) and the hole length constant and operated the system at 5 bar operating pressure. As presented in Figure 17, the maximum penetration depth

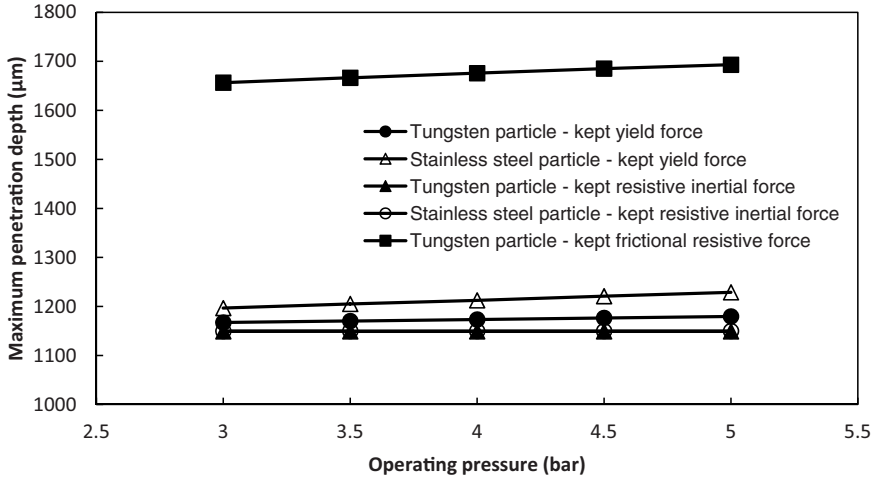

Figure 16. The effect of each resistive force on the maximum penetration depth of microparticles (stainless steel particle: 18 μm diameter; tungsten particle: 3 μm diameter; hole length: 1149 μm).

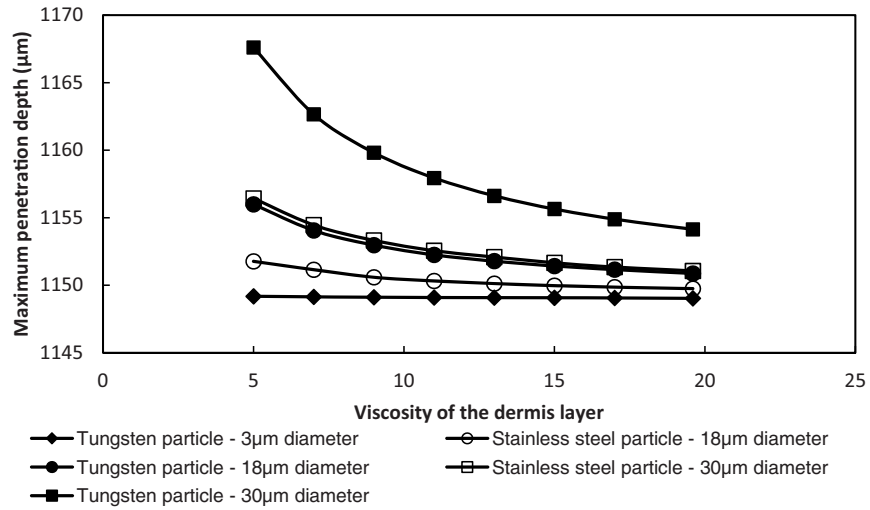

Figure 17. The effect of the viscosity of dermis layer on the maximum penetration depth of microparticles (operating pressure: 5 bar; hole length: 1149 μm).

decreased from an increase in viscosity of the dermis layer. This is because an increased resistive inertial force slows down the particle velocity rapidly. Figure 17 also shows that the effect of a decreased viscosity of dermis layer on the maximum penetration depth is increased from an increase in particle size and density due to an increased momentum. The maximum penetration depth of small microparticle (tungsten particle of 3 μm diameter) is kept to approximately a constant when the viscosity of dermis layers is changed.

Further discussions

A comparison between stainless steel and tungsten microparticles on the penetration depth in the skin mimicking agarose gel has been made in this study. Tungsten microparticles are unable to penetrate the skin mimicking agarose gel/skin without using MN in the experimental result, which is different from the results of stainless steel microparticles. The reason is that the diameter of tungsten microparticles is less than 1 μm, which is too small when compared with the stainless steel microparticles of 18 and 30 μm diameters. As a result, the momentum of the tungsten microparticles is too low to allow the particles to breach the gel surface. Zhang et al. (2013a) measured the velocity of ground slide, which only reaches around 122 m/s at 5 bar pressure, using a photoelectric sensor, which means that the particle velocity is less due to the energy loss. This velocity is less than some previous studies for gold particles, e.g. Kendall (2001) showed that 1 ± 0.2 μm diameter gold particles can reach a velocity of 580 ± 50 m/s at 40 bar pressure using a contoured shock tube (CST). The ground slide presents a significant negative effect on the particle velocity, but it has safety advantage that prevents the pressurized gas from impacting the human body. Thus, the operating pressure is mimicked from 3 to 60 bar to study the penetration differences of tungsten microparticles after increasing the momentum in the theoretical model. However, the tungsten microparticles still cannot achieve the expected penetration depth. It indicates that a ground slide-based gene gun system is not useful for the intercellular route because microparticles cannot reach velocities high enough to breach the skin. Increasing the particle size will increase the moment but cause damage to the surface of the skin. As a result, the extracellular route is the expected solution for normally ground slide-based gene gun system.

However, the use of MN meets the purpose of an intercellular route to deliver microparticle to a greater penetration depth in the target using a ground slide-based gene gun system. Previously, Zhang et al. (2013a) showed that the penetration depth of stainless steel microparticles is

increased while using an MN. In this study, the tungsten microparticles are investigated using modelling and experiments with MN-assisted microparticle delivery. Both model and experimental results show that the use of MN increases the penetration depth of tungsten microparticles. However, the maximum penetration depth of microparticles depends on the length of pierced holes which is created by MNs. The maximum penetration of tungsten microparticles reaches around 1149 μm using Adminpatch 1500 MM, which has possibly never reached for other relevant gene gun systems. For example, Kendall (2001) has indicated that gold particles of 1 ± 0.2 μm diameters can penetrate 66 μm in the skin at velocity of 580 ± 50 m/s using a CST. Kendall et al. (2004) also used a convergent–divergent device to accelerate 1.8 μm diameter gold particles that achieves a maximum penetration depth of 78.6 μm at 60 bar. Mitchell et al. (2003) showed that gold particles of 1–3 μm diameters can reach a maximum depth of around 60 μm in canine tissue at a velocity of 550 ± 50 m/s. It is concluded that the diameters of gold particles ranges from 1 to 3 only can penetrates to a depth from 60 to 78.6 μm (epidermis layer), which is less than the maximum penetration depth of the tungsten particles after using MNs. It shows that the improvement of the penetration depth using MN-assisted microparticle delivery, which achieves depths never reached before. In conclusion, the results show that the intercellular route is feasible for the MN-assisted microparticle delivery. In theory, it is the preferred route for MN-assisted microparticle delivery because the cell damage is minimized from a decrease in particle size (O'Brien & Lummis, 2011), although extracellular route presents more penetration depth. It could be proved by firing the above stainless steel/tungsten microparticles into cell cultured skin mimicking agarose gel to analyze the cell damage in further work. Future work should also focus on using animal/human skin for detailed histological studies in contrast to agarose gel as used in this study. If using the proposed methods, one should also be aware of the likeliness of dermal damage and pain that may occur if using long MNs besides any effect of gene gun on mechanical damage of the skin. Therefore, safety studies should be conducted in detail in future studies.

Conclusions

This study shows an effective method for relating the use of MNs to create holes on the target for microparticle delivery to improve the penetration depth of microparticles. The experimental rig considers possible changes in the operating pressure to analyze the penetration depth and passage percentage of tungsten and stainless steel microparticles. Results show that the passage percentage increases due to an increase in operating pressure until a maximum value. Tungsten microparticles used in this study present a lower passage percentage than stainless steel due to an insufficient momentum to reach the target (particle collector). In addition, tungsten microparticles are stopped by the skin mimicking agarose gel even if the operating pressure is increased. But an increased operating pressure improves the penetration of stainless steel particle without using MNs. This is because the diameter of tungsten microparticles is small (<1 μm). To further understand the effect of particle size and density on the penetration depth, a theoretical model is used to mimic the operating pressure ranges from 3 to 60 bar to accelerate tungsten and stainless steel microparticles while the diameter ranges from 3 to 100 μm. The results show a great improvement in the penetration depth of tungsten microparticles which is more than stainless steel microparticles. However, both model and experimental results show that a use of MNs provides an improvement on the penetration although the momentum is insufficient to breach the skin. The maximum penetration depth of microparticles up to dermis layer has not been reached before. It is related to length of MNs which determines the length of pierced holes. As expected, model results match well with the experimental results, which illustrate the applicability of the model for the MN-assisted microparticle delivery. MN-assisted microparticle delivery improves safety because an intercellular route can be chosen to reduce the damage from particle impact and the pressurized gas is prevented by the ground slide. In addition, it also enhances the penetration depth of microparticles properly when compared with any other gene gun systems. An increased penetration depth allows deeper tissue to be transfected, which provides more effective gene transfection in the target. Future work could be to attach the genes on the microparticles, fired into the cells using MN-assisted microparticle delivery and then to analyze the DNA profile of the cells to verify the advantage of MN-assisted microparticle delivery.

Acknowledgements

Loughborough University (UK) is acknowledged for providing a PhD studentship to Dongwei Zhang, which made this work possible. Furthermore, the technical supports from Mr Tony Eyre, Mr Mark Barron, Mr Jim Muddimer, Mr Terry Neale and Mr Steve Bowler are acknowledged.

Declaration of interest

The authors declare no conflict of interest.

References

- Al-Qallaf B, Das DB, Davidson A. (2009). Transdermal drug delivery by coated microneedles: geometry effects on drug concentration in blood. Asia-Pacific J Chem Eng 4:845–57.
- Arora A, Prausnitz MR, Mitragotri S. (2008). Micro-scale devices for transdermal drug delivery. Int J Pharm 364:227–36.
- Bastian S, Busch W, Kuhnel D, et al. (2009). Toxicity of tungsten carbide and cobalt-doped tungsten carbide nanoparticles in mammalian cells in vitro. Environ Health Perspect 117:530–6.
- Bennett AM, Phillpotts RJ, Perkins SD, et al. (1999). Gene gun mediated vaccination is superior to manual delivery for immunisation with DNA vaccines expressing protective antigens from Yersinia pestis or Venezuelan Equine Encephalitis virus. Vaccine 18:588–96.
- Crozier WD, Hume W. (1957). High velocity light gas gun. J Appl Phys 28:892–5.
- Cormier M, Johnson B, Ameri M, et al. (2004). Transdermal delivery of desmopressin using a coated microneedle array patch system. J Control Release 97:503–11.
- Davis SP, Landis BJ, Adams ZH, et al. (2004). Insertion of microneedles into skin: measurement and prediction of insertion force and needle fracture force. J Biomech 37:1155–63.
- Dehn J. (1987). A Unified theory if penetration. Int J Impact Eng 5: 239–48.

Duck FA. (1990). Physical properties of tissue: a comprehensive reference book. London: Academic Press, Harcourt Brace Jovanovich.

Donnelly RF, Garland MJ, Singh TRR, et al. (2012). Hydrogel-Forming microneedle array for enhanced transdermal drug delivery. Adv Funct Mater 22:4879–90.

Vexler A, Polyansky I, Gorodetsky R. (1999). Evaluation of skin viscoelasticity and anisotropy by measurement of speed of shear wave propagation with viscoelasticity skin analyser. J Invest Dermatol 113: 732–9.

Giudice EL, Campbell JD. (2006). Needle-free vaccine delivery. Adv Drug Deliv Rev 58:68–89.

Han T, Das DB. (2013). Permeability enhancement for transdermal delivery of large molecule using low-frequency sonophoresis combined with microneedles. J Pharmaceut Sci 102:3614–22.

Hardy MP, Kendall MAF. (2005). Mucosal deformation from an impinging transonic gas jet and the ballistic impact of micro-particles. Phys Med Biol 50:4567–80.

Holbrook KA, Odland GF. (1974). Regional Differences in the thickness (cell layers) of the human stratum corneum: an ultrasound analysis. J Invest Dermatol 62:415–22.

Kalluri H, Banga AK. (2011). Formation and closure of microchannels in skin following microporation. Pharm Res 28:82–94.

Kendall MAF, Carter FV, Mitchell TJ, Bellhouse BJ. (2001). Comparison of the transdermal ballistic delivery of micro-particle into human and porcine skin. Proceedings of the 23rd Annual International Conference of the IEEE; Istanbul, Turkey, 2991–94.

Kendall MAF, Rishworth S, Carter F, Mitchell T. (2004). Effects of relative humidity and ambient temperature on the ballistic delivery of micro-particles to excised porcine skin. J Invest Dermatol 122: 739–46.

Kis EE, Gerhard W, Myschik J. (2012). Devices for intradermal vaccination. Vaccine 30:523–38.

Kishino A, Yanagida T. (1988). Force measurements by micromanipulation of a single actin filament by glass needles. Nature 334:74–6.

Klein TM, Wolf ED, Wu R, Sanford JC. (1987). High-velocity microprojectiles for delivering nucleic acids into living cells. Nature 327:70–3.

Liu Y. (2006). Physical-mathematical modelling of fluid and particle transportation for DNA vaccination. Int J Eng Sci 44:1037–49.

Liu Y. (2007). Impact studies of high-speed micro-particle following biolistic delivery, IEEE transactions of biomedical engineering. Trans Biomed Eng 54:1507–13.

Macklin MD, Drape RJ, Swain WF. (2000). ''Preparation for particle-mediated gene transfer using the Accell gene gun. Methods Mol Med 29:297–303.

Matteucci, M, Fanetti, M, Casella, M, et al. (2009). Poly vinyl alcohol re-usable masters for MN replication. Microelectron Eng 86:752–6.

McAllister DV, Wang PM, Davis SP, et al. (2003). Microfabricated needles for transdermal delivery of macromolecules and nanoparticles: fabrication methods and transport studies. PNAS 100:13755–60.

Menezes V, Mathew Y, Takayama K, et al. (2012). Laser plasma jet driven microparticles for DNA/drug delivery. PLOS ONE, 7:e50823.

Mitchell TJ, Kendall MAF, Bellhouse BJ. (2003). A ballistic study of micro-particle penetration to the oral mucosa. Int J Impact Eng 28: 581–99.

Miyano T, Tobinaga Y, Kanno T, et al. (2005). Sugar micro needles as transdermic drug delivery system. Biomed Microdevices 7:185–8.

Nayak A, Das DB. (2013). Potential of biodegradable microneedles as a transdermal delivery vehicle for lidocaine. Biotechnol Lett 35: 1351–63.

Nayak A, Das DB, Vladisavljević GT. (2013). Microneedle-assisted permeation of lidocaine carboxymethylcellulose with gelatine co-polymer hydrogel. Pharmaceut Res. doi: 10.1007/s11095-013-1240-z (in press).

O'Brien JA, Lummis SCR. (2011). Nano-biolistics: a method of biolistic transfection of cells and tissues using a gene gun with novel nanometer-sized projectiles. BMC Biotechnol 11:66.

Olatunji O, Das DB. (2010). Painless Drug delivery using microneedles. In: Joan Escober Chavez, ed. Current technologies to increase the transdermal delivery of drugs. Bentham Science Publishers (available online at http://www.benthamdirect.org/pages/b_getarticleby-book.php). ISBN:978-1-60805-191-5.

Olatunji O, Das DB. (2011). Drug delivery using Microneedles. In: Zhanfeng Cui, ed. Comprehensive biotechnology. 2nd ed. MS number 501. Oxford, United Kingdom: MRW, Elsevier. ISBN: 13:978-0-444-53352-4.

Olatunji O, Das DB, Nassehi V. (2012). Modelling transdermal drug delivery using microneedles: effect of geometry on drug transport behavior. J Pharmaceut Sci 101:164–75.

Olatunji O, Das DB, Garland MJ, et al. (2013). Influence of array interspacing on the force required for successful microneedle skin penetration: theoretical and practical approaches. J Pharmaceut Sci 102:1209–21.

Quinlan NJ, Kendall MAF, Bellhouse BJ, Ainsworth RW. (2001). Investigations of gas and particle dynamics in first generation needle-free drug delivery device. Shock Waves 10:395–404.

Ritman EL. (2004). Micro-computed tomography – Current status and developments. Ann Rev Biomed Eng 6:185–208.

Russell JA, Roy MK, Sanford JC. (1992). Physical trauma and tungsten toxicity reduce the efficiency of biolistic transformation. Plant Physiol 98:1050–6.

Sato H, Hattori S, Kawamoto S, et al. (2000). In vivo gene gun-mediated DNA delivery into rodent brain tissue. Biochem Biophys Res Commun 270:163–70.

Schaefer H, Redelmeier TE. (1996). Skin barrier: principles of percutaneous absorption. New York: Karger.

Soliman SM. (2011). Micro-particle and gas dynamics in an axi-symmetric supersonic nozzle, University of Cincinnati (Cincinnati, USA). Thesis for the degree of Doctor of Philosophy in Aerospace Engineering.

Soliman SM, Abdallah S. (2011). CFD investigation of powdered vaccine and gas dynamics in biolistic gun. Powder Technol 214: 135–42.

Soliman SM, Abdallah S, Gutmark E, Turner MG. (2011). Numerical simulation of microparticles penetration and gas dynamics in an axi-symmertric supersonic nozzle for genetic vaccination. Powder Technol 208:676–783.

Thomas JL, Bardou J, Mauchamp B, et al. (2001). A helium burst biolistic device adapted to penetrate fragile insect tissues. J Insect Sci 1:1–10.

Trainer AH, Alexander MY. (1997). Gene delivery to the epidermis. Human Mol Genet 6:1761–7.

Uchida M, Li XW, Mertens P, Alpar HO. (2009). Transfection by particle bombardment: delivery of plasmid DNA into mammalian cells using gene gun. Biochim Biophys Acta 1790:754–64.

Walters KA, Roberts MS. (2007). Dermatologic, cosmeceutic, and cosmetic development, therapeutic and novel approaches. Chapter 36. NY: CRC Press, 591–611.

Webster C. (1995). The Discovery of Boyle's law, and the concept of the elasticity of air in the seventeenth century. Arch Hist Exact Sci 2: 441–502.

Wildnauer RH, Bothwell JW, Douglas AB. (1971). Stratum corneum properties I. Influence of relative humidity on normal and extracted stratum corneum. J Invest Dermatol 56:72–8.

Williams RS, Johnston SA, Riedy M, et al. (1991). Introduction of foreign genes into tissues of living mice by DNA-coated micro-projectiles. Proc Natl Acad Sci USA 88:2726–30.

Xu F, Wen T, Seffen KA, Lu TJ. (2007). Characterization of thermomechanical behaviour of skin tissue – viscoelastic behavior. Proceedings of the World Congress on Engineering, 2: WCE; 2007; London, UK.

Yoshida Y, Kobayashi E, Endo H, et al. (1997). Introduction of DNA into rat liver with a hand-held gene gun: distribution of the expressed enzyme, [32P] DNA, and Ca2+ flux. Biochem Biophys Res Commun 234:695–700.

Yoshimisu Y, Tanaka K, Tagawa T, et al. (2009). Improvement of DNA/metal particle adsorption in tungsten-based biolistic bombardment: alkaline pH is necessary for DNA adsorption and suppression of DNA degradation. J Plant Biol 52:524–32.

Zhang DW, Das DB, Rielly CD. (2013a). An experimental study of microneedles assisted micro-particle delivery using a model system. J Pharmaceut Sci 102:3632–44.

Zhang DW, Das DB, Rielly CD. (2013b). Potential of microneedles assisted micro-particles delivery from gene gun: a review. Drug Delivery. doi: 10.3109/10717544.2013.864345 (in press).

Zhang DW, Das DB, Rielly CD. (2014). Microneedles assisted micro-particles delivery from gene guns: experiments using skin mimicking agarose gel. J Pharmaceut Sci 103:613–27.